X-ray transitions associated with electron capture into bare dysprosium

1993 J. Phys. B: At. Mol. Opt. Phys. 26 1557

(http://iopscience.iop.org/0953-4075/26/9/004)

J. Phys. B: At. Mol. Opt. Phys. 26 (1993) 1557–1567. Printed in the UK

X-ray transitions associated with electron capture into bare dysprosium

H F Beyer†, K D Finlayson†, D Liesen†, P Indelicato‡, C T Chantler§, R D Deslattes§, J Schweppe§, F Bosch†, M Jung†, O Klepper†, W König†, R Moshammer†, K Beckert†, H Eickhoff†, B Franzke†, A Gruber†, F Nolden†, P Spädtke† and M Steck†

† Gesellschaft für Schwerionenforschung, GSI, Postfach 110552, D-6100 Darmstadt, Federal Republic of Germany

‡ Laboratoire de Physique Atomique et Nucléaire, Institut de Radium, Université Pierre et Marie Curie, T12, Boîte 93, 75252 Paris, Cedex 05, France

§ National Institute of Standards and Technology, Gaithersburg, MD 20899, USA

Received 6 October 1992, in final form 11 March 1993

Abstract. The Lyman and Balmer series in hydrogen-like Dy^{65+}, along with radiative electron capture (REC) into bare Dy^{66+}, have been observed. The x-ray spectra were measured in coincidence with one-electron capture in a beam of 292 MeV amu^{-1} Dy^{66+} stored in the ESR storage ring and interacting with an internal argon gas target. The REC line profile was studied in detail and was found to be in good agreement with theory, thus suggesting additional possibilities for spectroscopy.

1. Introduction

X-ray spectroscopy of few-electron heavy ions can be used to infer the radiative corrections to the binding energies of electrons in the strong field of a heavy nucleus (see, for instance, Kugel and Murnick 1977 or Brodsky and Mohr 1978). As opposed to many-electron atoms, the complication of electron correlation and shielding is avoided in one-electron ions. The quality of such measurements is largely dependent on how the few-electron ions are generated. A number of inherent problems have been encountered in precision experiments in the past, among these being the simultaneous population of spectator-electron states and the Doppler corrections associated with moving sources (Richard *et al* 1984, Beyer *et al* 1985). It should be possible (Deslattes *et al* 1984), using an ion storage ring employing ion cooling, to overcome the two main problems mentioned. In such an experiment (Beyer *et al* 1987) bare ions would be stored, cooled and decelerated, and the hydrogen-like states populated by single electron capture. The feasibility of such a scheme was previously demonstrated at the UNILAC at GSI in a single-pass experiment (Beyer *et al* 1991). Ultimately, the experiment has to achieve high spectral resolution which, because of the associated low detection efficiency, requires the full capabilities of the accelerator facility.

In the present publication we report on x-ray measurements performed at the internal gas target of the new 'Experimentierspeicherring' (ESR) at GSI. The experiment was conducted parasitically to the measurement of the bound-state beta decay of $^{163}Dy^{66+}$ (Jung *et al* 1992) as one of the first experiments after commissioning of the ESR. As the design goals

0953-4075/93/091557+11$07.50

of the ESR are not yet fully reached, intensities are still too low to afford the use of Bragg crystal-diffraction spectrometry. Instead, an intrinsic germanium Ge(i) detector was used. One advantage of such a detector is the large spectral region that can be monitored simultaneously. At a typical ion velocity of about 65% of the speed of light the Doppler effect is very large and correcting for it requires a precise knowledge of the observation angle. In the present work it was possible to partly avoid addressing the problem directly even without varying the ion-beam energy (Deslattes *et al* 1985). For this purpose we used, as an input, the theoretically calculated energy difference between the Lyman-α lines and the K-REC line. This energy is independent of the K-shell binding energy. A careful analysis of the REC line profile enabled us to determine this interval with a precision of a few times 10^{-4}, resulting in an accuracy approaching the same level for the 1s binding energy of Dy^{65+}. In addition, experimental cross sections have been obtained, knowledge of which is essential for the further development of the experimental programme.

2. Experimental details

The experimental arrangement, which is schematically illustrated in figure 1, is similar to that used in two earlier experiments (Finlayson *et al* 1992) conducted with neon and gold projectiles. Fully stripped Dy^{66+} ions at a specific energy of 292 MeV amu^{-1} were accumulated in the ESR with peak electrical currents approaching 1 mA. It was possible to maintain an internal argon gas jet with a thickness of 6×10^{12} cm^{-2}. The main experiment (Jung *et al* 1992), however, used the gas target only for short periods of typically 10 min for ionizing any hydrogen-like holmium projectiles produced during stacking. Between these periods with the gas on were longer periods of about 30 min length during which holmium was bred from the dysprosium nuclei via the process of beta decay.

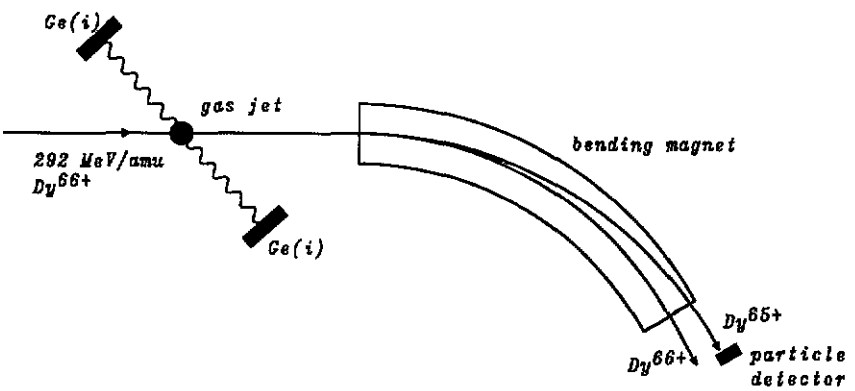

Figure 1. Schematic view of the experiment. The Ge(i) x-ray detector was placed at two different positions to measure x-rays under observation angles of approximately 132 and 48° relative to the ion-beam direction. Ions which captured an electron in the argon gas jet were registered in the particle detector.

The collimation of the gas jet was checked by moving the ion-beam orbit in the horizontal plane while noting the detection rate of hydrogen-like dysprosium ions in a position-sensitive multi-wire proportional counter (MWPC) (Klepper *et al* 1992) located

downstream of the target after the next ESR bending magnet. During the accumulation of spectra, x-rays emitted from the target region were measured in delayed coincidence with hydrogen-like ions in this particle detector. The Ge(i) detector could be mounted in front of two different ports of the vacuum chamber which were equipped with beryllium x-ray windows. The corresponding observation angles were $132.02 \pm 0.15°$ and $47.82 \pm 0.15°$ as measured by mechanical alignment. The Ge(i) detector, with an active area of 500 mm^2 and a thickness of 10 mm, had a FWHM energy resolution of 0.60 keV at x-ray energies near 120 keV. The x-ray detector and the electronics were carefully calibrated with radioisotopes of ^{57}Co, ^{133}Ba, ^{182}Ta and ^{241}Am. Procedures were adopted similar to those used in establishing secondary gamma-ray standards with solid-state detectors (Helmer *et al* 1975). Special care was taken in the modelling of the gamma-ray line profiles in order to determine a precise energy scale. It was possible to monitor the calibration continuously during the experiment by locating a very weak source of ^{241}Am near the detector. We observed run-to-run drifts of the order of 10 eV. The sum, however, of a large number of spectra turned out to be shifted only insignificantly. CAMAC electronics were used to record our data in list mode format. A timing signal derived from the Ge(i) detector was used to start a time-to-amplitude converter which was stopped by an anode signal from the MWPC. The combined timing resolution of x-ray plus particle detector was $\approx$ 15 ns. Offline analysis allowed the accumulation of data into separate spectra of coincident and non-coincident events.

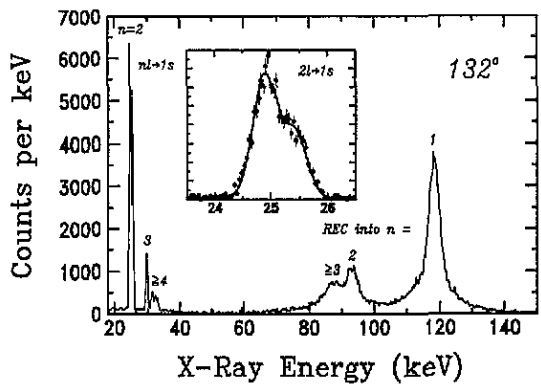

Figure 2. True coincident x-ray spectrum measured at 132°. Prominent lines arise from the $nl \rightarrow 1s$ Lyman series in hydrogen-like dysprosium and from REC into the low-lying states of Dy^{65+}.

3. Results and discussion

Measured x-ray spectra are shown in figures 2 and 3 where the very small background of random coincidences is already subtracted. Prominent features include the Lyman lines corresponding to $nl \rightarrow 1s$ transitions with $n = 2$, 3 and 4, and, in the case of the 132° observation, the radiative electron capture (REC) lines. In the forward direction, the latter are Doppler shifted to high energies out of the useful energy range of our detector. The insets show the Lyman-α doublet in more detail. In the spectrum taken at 132° the components are not as well resolved as they are at 48°. However, in the 132° direction an order of magnitude more counts were collected due to a longer acquisition time. The intensity

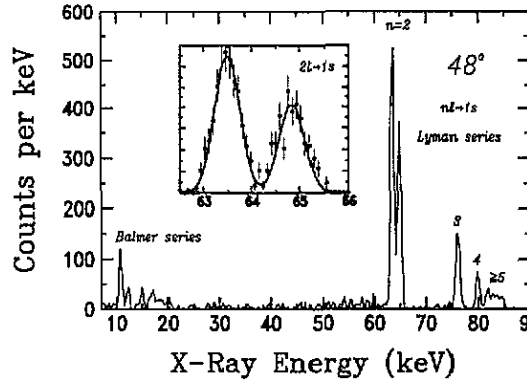

Figure 3. X-ray spectra measured under 48°. The prominent lines arise from the Lyman series in hydrogen-like dysprosium.

ratio in the $n = 2$ doublet is opposite to that found in the normal Kα spectrum of singly ionized dysprosium. Hence there must be a strong 2s component. The Balmer series is only visible in the blue-shifted spectrum of figure 3. At both observation angles we observe very clean hydrogen-like spectra on an extremely low background, as was demonstrated in the two previous experiments (Finlayson *et al* 1992) conducted with both lower beam current and lower gas thickness. What background there remains may still be associated with dysprosium x-rays. For quasi-free-electron bremsstrahlung (Yamadera *et al* 1981, Jackson 1967) one can expect a cross section falling off inversely with the photon energy giving rise to a background level of $\sim$ 1% under the strong lines. This is further suppressed by more than five orders of magnitude through the coincidence with the electron capture process. For the 2s state, the intensity ratio of its M1 compared with its 2E1 decay increases approximately with Z^4 (Drake 1988). At a nuclear charge of $Z = 66$ the 2s state, having a lifetime of 2.2×10^{-13} s, predominantly decays via its M1 branch. However, for about one-fifth of the time it still decays by the two-photon 2E1 emission. This might explain the small continuum background seen in figure 3 below the Lyman-α energy. The first few lines out of the Balmer series can also be identified in the same spectrum. However, the spectral resolution and statistical precision does not allow a quantitative analysis of their fine-structure components.

3.1. Radiative electron capture

At present high collision energy radiative electron capture (REC) is an important capture mechanism (Schnopper *et al* 1972, Spindler 1979). In this process a radiative transition of an initial target electron into a final projectile state occurs. The centre of the line appears near an energy of $T_r + |E_p| - \gamma|E_t|$, where T_r denotes the kinetic energy of an electron travelling with the same velocity (βc) as the projectile, and E_t and E_p are the initial- and final-state binding energies, respectively. As usual, γ, β and c denote the relativistic parameters and the velocity of light, respectively. The effect of the initial binding of the electron to the target is to broaden the REC x-ray line into a distribution with finite width. Within the impulse approximation, one assumes the initial states to be unperturbed target atomic states (Kleber and Jakubassa 1975, Kienle *et al* 1973). The double-differential cross section for REC may be written as

$$\frac{\partial^2\sigma^{\mathrm{REC}}}{\partial\Omega\partial E_{\mathrm{x}}} = \sum_{nl}\int \mathrm{d}^3\boldsymbol{p}_e|\Phi_{nl}(\boldsymbol{p}_e)|^2 2(2l+1)\frac{\partial\sigma^{\mathrm{f}}}{\partial\Omega}\delta(E_{\mathrm{x}} - (|E_{\mathrm{p}}| - \gamma|E_{\mathrm{t}}| + T_{\mathrm{r}} - \gamma\beta c p_{ez})) \qquad (1)$$

where the sum runs over all target nl subshells, and $\partial\sigma^{\mathrm{f}}/\partial\Omega$ is the differential cross section for the radiative capture of a free electron. E_{x} denotes the photon energy and $\Phi_{nl}(\boldsymbol{p}_e)$ the initial electron wavefunction in momentum space. p_{ez} represents the projection of the electron momentum onto the direction of the collision velocity. The integration is performed over all initial electron momenta $\boldsymbol{p}_e$ where the delta function takes care of the energy conservation by the photon emission (Kleber and Jakubassa 1975, Mokler *et al* 1991). The factor $2(2l+1)$ is the number of electrons per subshell. Equation (1) may be written as (cf Kleber and Jakubassa 1975)

$$\frac{\partial^2\sigma^{\mathrm{REC}}}{\partial\Omega\partial E_{\mathrm{x}}} = \frac{1}{\gamma\beta c}\frac{\partial\sigma^{\mathrm{f}}}{\partial\Omega}\mathcal{J}(p_{ez}) \qquad (2)$$

where $\mathcal{J}(p_{ez})$ denotes the Compton profile of the target atom which is the probability for finding the momentum component p_{ez}. For $\partial\sigma^{\mathrm{f}}/\partial\Omega$ we used the formulae given by Stobbe (1930). The Compton profiles $\mathcal{J}(p_{ez})$ were computed using spherically averaged wavefunctions $\Phi_{nl}(p_e)$. For this purpose, Clementi and Roetti (1974) double-zeta functions were generated using Fourier-transformed Slater-type basis functions. Our calculated Compton profiles are in excellent agreement with the experiment of Eisenberger and Reed (1972) and also with the calculations of Biggs *et al* (1975). For the asymptotic behaviour at large momenta we obtain a perfect coincidence with the calculation of Westgate *et al* (1991).

The calculated double-differential cross sections for radiative capture into the dysprosium K shell are plotted in figure 4 where the individual contributions from the argon-target subshells are given in addition to the summed cross section. In figure 4 the abscissa is the x-ray energy in the emitter frame of reference minus the absolute value of the projectile binding energy, E_{p}. To evaluate the x-ray energies according to equation (1) we used tabulated values for the target binding energies, E_{t}, found in the literature (Bearden and Burr 1967, Cauchois and Senemaud 1978). For radiative capture into the L, M and higher shells the calculations are identical apart from the different projectile binding energies and free-electron capture cross sections.

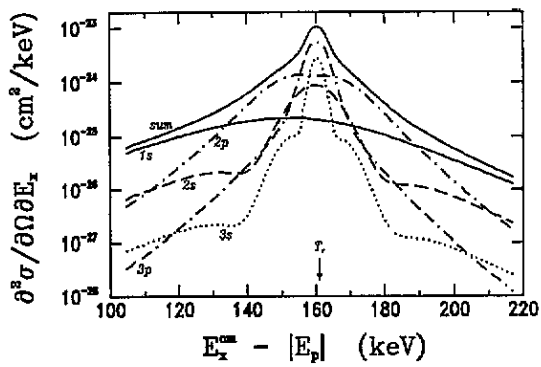

Figure 4. Calculated double-differential cross section for REC into the dysprosium K shell. The contributions of the argon subshells and their total sum are also shown.

Of course, the Compton profiles are symmetric in p_{ez} and also in the x-ray energy, E_x, due to its linear dependence on p_{ez}. The skewness of the summed REC line observable in figure 4 is attributable to two effects. First, the contributions from the different target orbitals are located at different positions according to their binding energies. Second, the individual contributions exhibit a skewness due to the decrease of the REC cross section with photon energy. The latter effect cannot be avoided even in a one-electron target. The result is a noticeable centroid shift to lower x-ray energies relative to the position $(T_r - \gamma|E_t|)$ predicted if the profile were symmetric. Even for loosely bound 3p electrons the shift amounts to -190 eV in the emitter frame of reference, indicating that the effect cannot be neglected even in lighter targets such as hydrogen. The summed theoretical cross section was transformed into the laboratory frame and subsequently convoluted with a (normalized) 'experimental' monochromatic detection line profile in order to be able to compare the calculations with the measurements. In order to obtain a realistic profile a Monte Carlo simulation (Finlayson 1992) was performed to simulate the fast-beam x-ray source while taking into account the geometry and the measured ion-beam parameters. A Gauss function was taken to approximate the Ge(i) response function with a measured FWHM of 0.60 keV. The resulting simulated detection line profile was found to be consistent with the shape observed in the Lyman lines.

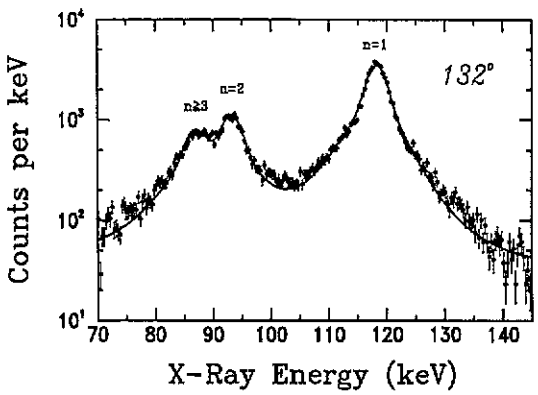

Figure 5. Experimental REC spectrum (data points) and theoretical fit (full line).

The convoluted theoretical curve was used as a fit function, the absolute energy position and the absolute height being the only two free parameters. From their fitted values the corresponding projectile binding energy, E_p, and the experimental cross section were extracted. In figure 5 the REC spectrum is displayed logarithmically, where the measurement is represented by the data points and the continuous curve shows the least-squares fit with the theoretical profiles. A remarkably good correspondence between experiment and theory is obtained. The skewness of the REC profile mentioned before is a critical point if one wishes to deduce inner-shell binding energies from the centroid of measured REC profiles. Mokler *et al* (1991) recently proposed REC as a tool for spectroscopy, neglecting such a centroid shift. Furthermore, they claimed that any centroid shift would *not* influence the REC energy extrapolated to zero collision energy. A strong argument against this is that the negative slope of the REC cross section persists down to zero energy. In the early work of Kienle *et al* (1973), considerable shifts to lower energies compared with theoretical estimates had already been reported, presumably with the underlying assumption

of a constant capture cross section over the line profile. In addition, one may question the validity of the impulse approximation (Jakubassa-Amundsen 1987) and speculate about systematic shifts caused by screening and off-shell effects (Gorriz *et al* 1983, Briggs and Dettmann 1974). Such phenomena would be most important at low collision velocities. However, in the present experiment, where the collision velocity is much higher than the Bohr velocity ($Z\alpha c$) of the target K electrons, the theoretical treatment should be adequate. Based on the theoretical energies given by Johnson and Soff (1985), our experimental REC profile lies (in the laboratory frame) only about 120 eV lower than the theoretical estimate. This is well within the experimental uncertainty in the Doppler correction due to uncertainties in projectile velocity and in observation angle.

3.2. Energies

We extracted the x-ray energies of the Lyman-α transitions by applying the Gauss fits represented by the continuous curves in the insets of figures 2 and 3. The lower-energy component of the doublet labelled $2l \rightarrow 1s$ arises from the unresolved sum of two transitions, $2s_{1/2} \rightarrow 1s_{1/2}$ and $2p_{1/2} \rightarrow 1s_{1/2}$. From the high relative intensity observed in this peak we can assume a dominant 2s component. This is also consistent with the REC capture mechanism favouring the $l = 0$ states. We can extract the $2s_{1/2} \rightarrow 1s_{1/2}$ transition energy with only a small correction for the presence of the $2p_{1/2} \rightarrow 1s_{1/2}$ component. In this procedure, we made use of an independently available estimate of the 2s Lamb shift amounting to 15.1 eV (Johnson and Soff 1985); it was also assumed that the $2p_{3/2}$ and $2p_{1/2}$ states were populated in the statistical 2:1 ratio and that the observed lineshapes can be approximated by Gauss functions. The correction can be calculated from the observed Lyman-α_1/Lyman-α_2 intensity ratio which amounts to 0.63 ± 0.07 and 0.52 ± 0.03 in the forward and backward directions, respectively. In a field-free environment all components should have the same angular dependence and thus constant intensity ratios, which seems to be roughly fulfilled within the statistical precision. The intensity ratio stated above (for 132°) implies a $2s_{1/2}$ / $2p_{1/2}$ ratio of 2.85 ± 0.22 leading to a correction of only (-3.9 ± 0.2) eV to the observed peak energy to yield the $2s_{1/2} \rightarrow 1s_{1/2}$ transition energy. We point out that the size of this correction is only weakly dependent on the assumptions made concerning the relative level populations.

Doppler corrections are needed to obtain experimental transition energies in the emitter frame of reference, i.e. the measured laboratory x-ray energies are multiplied by the factor

$$D(\beta, \theta) = \gamma(1 - \beta \cos\theta). \tag{3}$$

$D(\beta, \theta)$ amounts to ~ 0.74 and ~ 1.89 for $\theta = 48°$ and 132°, respectively. The beam velocity ($\beta = 0.6486(1)$) was measured by Schottky diagnostics yielding relative errors in $D(\beta, \theta)$ of 6×10^{-6} and 1.6×10^{-4} for the forward and backward angle, respectively. However, the largest error in $D(\beta, \theta)$ is due to the $\pm 0.15°$ angular uncertainty and emerges as 2×10^{-3} for the forward direction and as 9×10^{-4} for the backward direction. The Doppler factor (3) can also be determined from the ratio between a known energy interval in the emitter frame and its corresponding measured value in the laboratory frame. If one is interested in the radiative corrections to the 1s state this interval should be independent of the 1s binding energy. For such an interval one can use the energy difference between the Lyman-α doublet and the K-REC line. In this case the Doppler factor is

$$D(\beta, \theta) = \frac{\overline{E}_{x,\mathrm{kin}} - |E_L|}{\Delta E_{\mathrm{lab}}} \tag{4}$$

Table 1. Experimental Lyman-α energies in keV obtained by applying Doppler corrections at $47.82 \pm 0.15°$ and at $132.02 \pm 0.15°$ and, alternatively, by using the REC spectrum to determine the observation angle. The theoretical transition energies of Johnson and Soff (1985) are given for comparison.

	$\theta = 48°$	$\theta = 132°$	Using REC	Theory
$2s_{1/2} \rightarrow 1s_{1/2}$	47.096(110)	46.996(56)	47.022(38)	47.045
$2p_{3/2} \rightarrow 1s_{1/2}$	48.089(110)	47.994(56)	48.025(38)	48.038

Table 2. Error contributions to the K x-ray energies of Dy^{65+}.

Source of error	Error (eV)
Statistics	25
Beam velocity	7
Calibration	20
REC model	20
Total	38

where $\overline{E}_{x,kin}$, according to equation (1), is given by the calculated average $\overline{T_r - \gamma|E_t| - \gamma\beta c p_{ez}}$ over the K-REC profile, E_L denotes the binding energy of one of the L states (we chose the 2s) and ΔE_{lab} the measured energy difference.

Our extracted transition energies are summarized in table 1 where the second and third columns contain the results obtained with the mechanically determined observation angles and the fourth column the results from the 132° observation using the spectroscopically determined observation angle. In the last column the theoretical energies of Johnson and Soff (1985) are given. The errors quoted in table 1 reflect the superior quality of the data obtained at 132° due to higher statistical precision and lower sensitivity to angular uncertainties. The results also show a further improvement when the mechanical angular measurement is avoided. For this latter case the error contributions are listed in table 2. The main contributions arise from the statistical uncertainty and from the detector calibration. The results depend on the precise calculation of the REC profile as already discussed in the previous section. Therefore, we add a 20 eV error contribution (in quadrature) for residual model uncertainties. Such a small error seems to be justified because other theoretical treatments, as for instance the strong potential Born approximation (Gorriz *et al* 1983), will increase the size of the cross section by nearly a factor of four, but will only slightly alter the lineshape, implying insignificant centroid shifts. Our experimental results, obtained in three different ways, are all consistent within their quoted error bars. The energies derived from the 48° measurement are somewhat higher and the results from the 132° measurements somewhat lower than the more precise result using the REC line, with the scatter of the data being typically only 0.3 to 0.5 combined standard deviations. This seems to indicate that our observation angles are well within their estimated uncertainty. Indeed, the spectroscopically determined observation angle emerges as $132.19 \pm 0.06°$ and is in very good agreement with the quoted mechanical value of $132.02 \pm 0.15°$. As can be seen in table 1, our experiment is also in good agreement with the theory of Johnson and Soff (1985), both in absolute terms and with regard to the $2s_{1/2}$–$2p_{3/2}$ splitting. The latter differs only by 10 eV. Our error bars of ±38 eV are still too large for a stringent test of QED calculations since the radiative corrections to the 1s state in hydrogen-like dysprosium amount to only ~ 97 eV.

The present experiment has demonstrated that clean spectra of hydrogen-like ions can

be observed at the internal gas target of the ESR. The observed background level is very low. Allowing for further intensity improvements in the future, along with the anticipated deceleration capabilities of the storage ring, we expect considerable progress in the precision of this kind of experiment. Variation of the beam energy during an experiment (as already planned) will lead to a significant improvement in the accuracy of the Doppler correction. It will also help to remove possible small ambiguities in the theoretical model of the REC profile. Finally, we also plan to use a lighter target gas like helium. This will also narrow the REC lines.

3.3. Cross sections

Our results for the x-ray production cross sections per target atom are compiled in table 3. In the first part, the total cross sections are given for radiative capture into the K and L shells, and the integrated cross section for capture into the M and higher shells. In the second part the cross sections for the emission of the observed Lyman lines are given. For the determination of the absolute cross sections the x-ray detection efficiency, the ion-beam intensity, the efficiency of the particle detector and, most critically, the thickness of the argon gas jet are needed. Taking into account the systematic errors of all these quantities, we can estimate a total (systematic) uncertainty of about 50%. In table 3 the measured REC cross sections are compared with theoretical estimates obtained by using Stobbe's theory (1930) for the capture of a free electron and multiplying them with the number of target electrons. Such an approximation is valid (Briggs and Dettmann 1974) when the beam velocity (108 atomic units) is large compared with the nuclear charge of the target, which is nearly fulfilled in the present case. Calculations of radiative muon capture reported by Soff and Rafelski (1989) are in agreement with Stobbe's formulae if one replaces the reduced mass of the muon by the corresponding value of the electron. We used their computer program to estimate the integrated cross section for capture into shells with principal quantum numbers $n \geqslant 3$ summing the cross sections up to $n = 20$. For capture into the K shell good agreement is obtained between experiment and theory. For the L and M plus higher shells the differences are near 50% which is difficult to explain because our relative cross sections should be accurate to $\sim 10\%$.

Table 3. X-ray production cross sections given in cm^2 for 292 MeV amu^{-1} $Dy^{66+} \rightarrow Ar$. The experimental results are compared with estimates obtained with the theory of Stobbe (1930) for radiative capture of free electrons.

Process	Experiment ($\times 10^{-22}$)	Theory ($\times 10^{-22}$)
REC		
K	3.7	3.7
L	87	62
$\geqslant$M	65	41
Characteristic radiation	Experiment ($\times 10^{-22}$)	Expected from REC (expt) ($\times 10^{-22}$)
L $\rightarrow$ K	1.8	1.3
M $\rightarrow$ K	37	
N $\rightarrow$ K	14	
One-electron capture	0.11	5.2

The characteristic lines arise from both radiative and non-radiative capture into excited states and the subsequent cascade transitions. In the Lyman-α lines the whole L-REC intensity has to show up together with the cascade fraction from higher shells. Assuming an average cascade factor of 60% (Beyer *et al* 1987) for $n \geqslant 3$ and using the experimental cross sections one expects a Lyman-α cross section of 1.3×10^{-22} cm^2 as induced by radiative capture. This compares with the measured cross section of 1.8×10^{-22} cm^2 which is expected to contain additional contributions from non-radiative capture. In the last row of table 3 the total experimental one-electron capture cross section is compared with the sum of the measured radiative-capture cross sections. The difference of 5×10^{-22} may be attributed to the non-radiative capture. Using eikonal theory the $K \rightarrow K$ cross section, comprising the largest contribution in the non-radiative capture, has been estimated (Eichler 1985, Stöhlker 1992) to be 4×10^{-22} cm^2. This fits nicely with the experimental findings. In summary, our cross sections represent a consistent set of data which, apart from the few mentioned deviations in their relative magnitude, agree well with the theoretical estimates.

Acknowledgments

We enjoyed fruitful discussions with G Soff. Technical assistance by W Enders and by H Wesp is gratefully acknowledged.

References

Bearden J A and Burr A F 1967 *Rev. Mod. Phys.* **39** 125–42
Beyer H F, Deslattes R D, Folkmann F and LaVilla R E 1985 *J. Phys. B: At. Mol. Phys.* **18** 207–15
Beyer H F, Deslattes R D and Liesen D 1987 *Precision X-Ray Spectroscopy in One- and Two-Electron Heavy Ions: Proposal for an Experiment at the Experimental Storage Ring (ESR)* GSI Darmstadt
Beyer H F, Indelicato P, Finlayson K D, Liesen D and Deslattes R D 1991 *Phys. Rev.* A **43** 223–7
Biggs F, Mendelsohn L B and Mann J B 1975 *At. Data Nucl. Data Tables* **16** 201–309
Briggs J S and Dettmann K 1974 *Phys. Rev. Lett.* **33** 1123–5
Brodsky S J and Mohr P J 1978 *Structure and Collisions of Ions and Atoms* vol 3, ed I A Sellin (Berlin: Springer)
Cauchois Y and Senemaud C 1978 *International Tables of Selected Constants* vol 18 (Oxford: Pergamon)
Clementi E and Roetti C 1974 *At. Data Nucl. Data Tables* **14** 177–478
Deslattes R D 1984 *Workshop on the Physics with Heavy Ion Cooler Rings (Heidelberg, 29–30 May)*
Deslattes R D, Schuch R and Justiniano E 1985 *Phys. Rev.* A **32** 1911–3
Drake G W F 1988 *The Spectrum of Atomic Hydrogen—Advances* ed G W Series (Singapore: World Scientific) pp 137–241
Eichler J 1985 *Phys. Rev.* A **32** 112–21
Eisenberger P and Reed W A 1972 *Phys. Rev.* A **5** 2085–93
Finlayson K D 1992 *GSI Report* GSI-92-18 ISSN 0171-546
Finlayson K D *et al* 1992 to be published
Gorriz M, Briggs J S and Alston S 1983 *J. Phys. B: At. Mol. Phys.* **16** L665–70
Helmer R G, Cline J E and Greenwood R C 1975 *The Electromagnetic Interaction in Nuclear Spectroscopy* (Amsterdam: North-Holland)
Jackson J D 1967 *Classical Electrodynamics* (New York: Wiley)
Jakubassa-Amundsen D H 1978 *J. Phys. B: At. Mol. Phys.* **20** 325–36
Johnson W R and Soff G 1985 *At. Data Nucl. Data Tables* **33** 405–46
Jung M *et al* 1992 *Phys. Rev. Lett.* **69** 2164–7
Kienle P, Kleber M, Povh B, Diamond R M, Stephens F S, Grosse E, Maier M R and Proetel D 1973 *Phys. Rev. Lett.* **31** 1099–102
Kleber M and Jakubassa D H 1975 *Nucl. Phys.* A **252** 152–62
Klepper O *et al* 1992 *Nucl. Instrum. Methods* B **70** 427–33
Kugel H W and Murnick D E 1977 *Rep. Prog. Phys.* **40** 297–343

Mokler P H, Stöhlker Th, Kozhuharov C, Stachura Z and Warczak A 1991 *Z. Phys.* D **21** 197–200
Richard P, Stökli M, Deslattes R D, Cowan P, LaVilla R E, Johnson B, Jones K, Mann R, Schartner K-H and Meron M 1984 *Phys. Rev.* A **29** 2939–42
Schnopper H W, Betz H D, Delvaille J P, Kalata K, Sohval A R, Jones K W and Wegner H G 1972 *Phys. Rev. Lett.* **29** 898–901
Soff G and Rafelski J 1989 *Z. Phys.* D **14** 187–90
Spindler E 1979 *Thesis* University of München
Stobbe M 1930 *Ann. Phys., Lpz.* **7** 661–715
Stöhlker Th 1992 private communication
Westgate W M, Sagar R P, Farazdel A, Smith V H, Simas A M and Thakkar A 1991 *At. Data Nucl. Data Tables* **48** 213–9
Yamadera A, Ishi K, Sera K, Sebata M and Morita S 1981 *Phys. Rev.* A **23** 24–33